Interline Power Flow Controller Application for Low Frequency Oscillations Damping

ALIVELU, M. PARIMI IRRAIVAN ELAMVAZUTHI NORDIN SAAD
Department of Electrical and Electronic Engineering
Universiti Teknologi Petronas
Bandar Seri Iskander, 31750, Tronoh, Perak
MALAYSIA
alivelup@yahoo.co.in, irraivan_elamvazuthi@petronas.com.my, nordiss@petronas.com.my

Abstract: This paper presents the modeling of the power system installed with the Interline Power Flow Controller (IPFC), the latest proposed Flexible AC Transmission System (FACTS) controller. The IPFC is modeled in d-q axis form, and the dynamic model of a single machine infinite bus (SMIB) power system installed with IPFC is developed. Further, the linearized Phillips-Heffron model of the power system is established to study the oscillation stability. The damping controllers considering the various control signals are designed based on the linearized model. The power oscillation stability is investigated with the use of eigenvalue analysis and by nonlinear simulation of the dynamic model of the power system. Studies reveal that the most effective input signal of IPFC utilized for damping the low frequency oscillations is found to be the input signal m_2, providing robust performance under different operating conditions.

Key-Words: - FACTS, Interline power flow controller, Modelling, Phillips Heffron model, Power oscillation stability

1 Introduction

The phenomenon that is of great interest and vital concern in the power industry is the stability of electromechanical oscillations, i.e., the low frequency oscillations having an oscillation frequency in the range of 0.2 Hz to 2 Hz. These oscillations limit the maximum amount of power that can be transferred over the transmission lines and sometimes may have disastrous consequences to the interconnected systems stability, leading to partial or total collapses (black-outs). Therefore, equipment and procedures to enhance the damping of these oscillations become mandatory for the safe system operation, and to allow a better use of the existent transmission network. The traditional approaches to aid the damping of a power system oscillations is by adding a Power System Stabilizer (PSS) in the excitation system of the generator for which much experience and insight exist in the industry [1]-[3]. In the recent years, the rapid growth of power electronics has made Flexible AC Transmission Systems (FACTS) controllers very important in terms of controller application in power system damping in addition to their primary purpose of reactive power support, controlling line power flows etc. Major contributions have been made in [4]-[12], in damping of power system oscillations where universal approaches are proposed for the analysis of the FACTS devices such as Thyristor Controlled Series Capacitor (TCSC), Static Var Compensator (SVC), Static Synchronous Compensator (STATCOM), Static Synchronous Series Capacitor (SSSC), Unified Power Flow Controller (UPFC).

Interline Power Flow Controller (IPFC), is the latest representative of the Voltage Source Converter (VSC) based FACTS devices, and was proposed by Gyugyi with Sen and Schauder [13]. Like the UPFC, the IPFC is a combined compensator, consisting of at least two or more VSCs with a common dc link. This dc link provides the device with an active power transfer path among the converters, thereby facilitating real power transfer among the lines of the transmission system which enables the IPFC to compensate multiple transmission lines at a given substation. Each converter also provides reactive power compensation independently on its own transmission line. Thus, the IPFC provides the real and reactive power compensation to the system. The controllability of the line power flow by IPFC has been well recognized [14]-[16]. However, very limited information is reported [17]-[19] concerning the control of the IPFC to provide additional damping during system oscillations. The damping function of the IPFC has not been investigated thoroughly. Chen *et. al*. [17, 18], proposed a PID controller for oscillation damping enhancement in a SMIB test system. However, due to the complexity and nonlinearity of the power system the performance of the damping controller is degraded to a certain extent. Kazemi et. al [19] proposed a PI supplementary controller with its input equal to the electrical power of the generator for oscillation damping. However, they have not optimized the parameters of the controller.

In the view of this, the primary object of this paper is to develop a dynamic model for IPFC for small signal stability analysis and examine its damping function in mitigating the power system oscillations. The rest of the paper is organized as follows: Firstly the mathematical model has been developed for IPFC in d-q axis form in section 2. Secondly a small signal linearized Phillips–Heffron model of a power system installed with an IPFC is derived in section 3. Thirdly the IPFC based damping controller is designed on the basis of linearized system model, using the phase compensation method as described in section 4. Lastly the relative effectiveness of the IPFC control signals on which the damping function of the IPFC is superimposed is examined and analyzed on single machine infinite bus power system (SMIB). The performance of IPFC based controllers in achieving the damping of low frequency oscillations of the power system is compared. The effectiveness of the controllers under wide variations in operating conditions is studied. The ability of the damping controllers during various disturbances is examined with nonlinear simulation of the dynamic model of the power system. The simulation results are given in section 5.

2 Modeling of IPFC

The schematic diagram of IPFC is shown in Fig. 1. It consists of two three phase Gate turn-off (GTO) based VSCs, each providing series reactive compensation for the two lines. The VSCs are linked together at their dc terminals and are connected to the transmission lines through their series coupling transformers. The converters can transfer the real power between them via their common dc terminal. In Fig. 1, m_1, m_2 and δ_1, δ_2 refer to amplitude modulation index and phase-angle of the control signal of each VSC, respectively, which are the input control signals to the IPFC. To model the IPFC, consider phase '*a*' of the coupling transformer and the VSC 1, arms along with the dc link, as shown in Fig. 2. C_{dc} is the dc link capacitor. r_1 and l_1 are the per phase resistance and inductance of transformer on line 1. ς_{C1a} and ς'_{C1a} represent the bidirectional switches which can be either on or off in Fig. 2. r_s is the switch on state resistance.

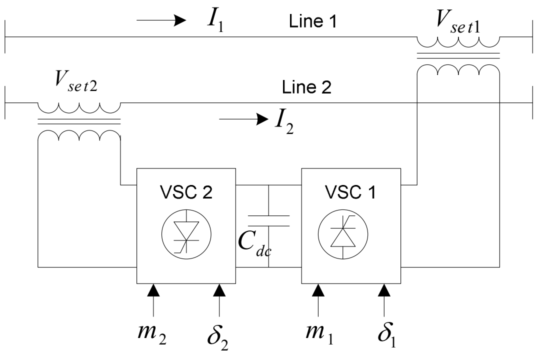

Fig. 1. Schematic diagram of IPFC

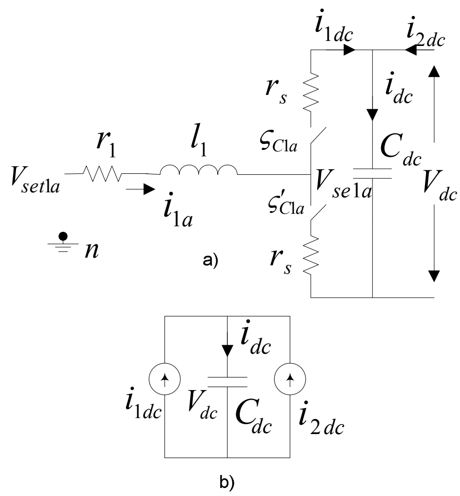

Fig. 2. a) Equivalent circuit of phase 'a' of coupling transformer and VSC 1. b) Dynamics of dc link capacitor.

The mathematical model for each phase a, b and c for both the VSC's are obtained similar to the approach in [20]. The three phase differential equations of the IPFC are:

$$\begin{bmatrix} \dfrac{di_{1a}}{dt} \\ \dfrac{di_{1b}}{dt} \\ \dfrac{di_{1c}}{dt} \end{bmatrix} = \begin{bmatrix} -\dfrac{R_1}{l_1} & 0 & 0 \\ 0 & -\dfrac{R_1}{l_1} & 0 \\ 0 & 0 & -\dfrac{R_1}{l_1} \end{bmatrix} \begin{bmatrix} i_{1a} \\ i_{1b} \\ i_{1c} \end{bmatrix} - \frac{m_1 v_{dc}}{2l_1} \times$$

$$\begin{bmatrix} \cos(\omega t+\delta_1) \\ \cos(\omega t+\delta_1-120^0) \\ \cos(\omega t+\delta_1-240^0) \end{bmatrix} + \begin{bmatrix} \frac{1}{l_1} & 0 & 0 \\ 0 & \frac{1}{l_1} & 0 \\ 0 & 0 & \frac{1}{l_1} \end{bmatrix} \begin{bmatrix} V_{set1a} \\ V_{set1b} \\ V_{set1c} \end{bmatrix} \tag{1}$$

$$\begin{bmatrix} \frac{di_{2a}}{dt} \\ \frac{di_{2b}}{dt} \\ \frac{di_{2c}}{dt} \end{bmatrix} = \begin{bmatrix} -\frac{R_2}{l_2} & 0 & 0 \\ 0 & -\frac{R_2}{l_2} & 0 \\ 0 & 0 & -\frac{R_2}{l_2} \end{bmatrix} \begin{bmatrix} i_{2a} \\ i_{2b} \\ i_{2c} \end{bmatrix} - \frac{m_2 v_{dc}}{2l_2} \times$$

$$\begin{bmatrix} \cos(\omega t+\delta_2) \\ \cos(\omega t+\delta_2-120^0) \\ \cos(\omega t+\delta_2-240^0) \end{bmatrix} + \begin{bmatrix} \frac{1}{l_2} & 0 & 0 \\ 0 & \frac{1}{l_2} & 0 \\ 0 & 0 & \frac{1}{l_2} \end{bmatrix} \begin{bmatrix} V_{set2a} \\ V_{set2b} \\ V_{set2c} \end{bmatrix} \tag{2}$$

where $R_1 = r_1 + r_s$. The dc link capacitor voltage is:

$$\frac{dv_{dc}}{dt} = \frac{m_1}{2C_{dc}} \left[\cos(\omega t+\delta_1) \ \cos(\omega t+\delta_1-120^0) \right.$$

$$\left. \cos(\omega t+\delta_1+120^0) \right] \begin{bmatrix} i_{1a} \\ i_{1b} \\ i_{1c} \end{bmatrix} + \frac{m_2}{2C_{dc}} \left[\cos(\omega t+\delta_2) \right.$$

$$\left. \cos(\omega t+\delta_2-120^0) \ \ \cos(\omega t+\delta_2+120^0) \right] \begin{bmatrix} i_{2a} \\ i_{2b} \\ i_{2c} \end{bmatrix} \tag{3}$$

2.2 IPFC modeled in d-q axis form

By applying the Park's transformation, the equations (1-3) are developed into the rotating reference ($d-q-o$ axis) frame as:

$$\begin{bmatrix} \frac{di_{1d}}{dt} \\ \frac{di_{1q}}{dt} \\ \frac{di_{10}}{dt} \end{bmatrix} = \begin{bmatrix} -\frac{R_1}{l_1} & \omega & 0 \\ -\omega & -\frac{R_1}{l_1} & 0 \\ 0 & 0 & -\frac{R_1}{l_1} \end{bmatrix} \begin{bmatrix} i_{1d} \\ i_{1q} \\ i_{10} \end{bmatrix} + \begin{bmatrix} \frac{1}{l_1} & 0 & 0 \\ 0 & \frac{1}{l_1} & 0 \\ 0 & 0 & \frac{1}{l_1} \end{bmatrix} \begin{bmatrix} v_{set1d} \\ v_{set1q} \\ v_{set10} \end{bmatrix}$$

$$-\frac{m_1 v_{dc}}{2l_1} \begin{bmatrix} \cos\delta_1 \\ \sin\delta_1 \\ 0 \end{bmatrix} \tag{4}$$

$$\begin{bmatrix} \frac{di_{2d}}{dt} \\ \frac{di_{2q}}{dt} \\ \frac{di_{20}}{dt} \end{bmatrix} = \begin{bmatrix} -\frac{R_2}{l_2} & \omega & 0 \\ -\omega & -\frac{R_2}{l_2} & 0 \\ 0 & 0 & -\frac{R_2}{l_2} \end{bmatrix} \begin{bmatrix} i_{2d} \\ i_{2q} \\ i_{20} \end{bmatrix} + \begin{bmatrix} \frac{1}{l_2} & 0 & 0 \\ 0 & \frac{1}{l_2} & 0 \\ 0 & 0 & \frac{1}{l_2} \end{bmatrix} \begin{bmatrix} v_{set2d} \\ v_{set2q} \\ v_{set20} \end{bmatrix}$$

$$-\frac{m_2 v_{dc}}{2l_2} \begin{bmatrix} \cos\delta_2 \\ \sin\delta_2 \\ 0 \end{bmatrix} \tag{5}$$

$$\frac{dv_{dc}}{dt} = \frac{3m_1}{4C_{dc}} \left[\cos\delta_1 \ \ \sin\delta_1 \ \ 0 \right] \begin{bmatrix} i_{1d} \\ i_{1q} \\ i_{10} \end{bmatrix} + \frac{3m_2}{4C_{dc}} \left[\cos\delta_2 \ \ \sin\delta_2 \ \ 0 \right] \begin{bmatrix} i_{2d} \\ i_{2q} \\ i_{20} \end{bmatrix} \tag{6}$$

Equations (4-6) represent the three phase dynamic differential equations of the IPFC on the rotor axis frame. Neglecting the resistance and transients of series converter transformers the dynamic model of IPFC (4-6) can be written as:

$$\begin{bmatrix} V_{set1d} \\ V_{set1q} \end{bmatrix} = \begin{bmatrix} 0 & -x_{t1} \\ x_{t1} & 0 \end{bmatrix} \begin{bmatrix} i_{1d} \\ i_{1q} \end{bmatrix} + \frac{v_{dc}}{2} \begin{bmatrix} m_1 \cos\delta_1 \\ m_1 \sin\delta_1 \end{bmatrix} \tag{7}$$

$$\begin{bmatrix} v_{set2d} \\ v_{set2q} \end{bmatrix} = \begin{bmatrix} 0 & -x_{t2} \\ x_{t2} & 0 \end{bmatrix} \begin{bmatrix} i_{2d} \\ i_{2q} \end{bmatrix} + \frac{v_{dc}}{2} \begin{bmatrix} m_2 \cos\delta_2 \\ m_2 \sin\delta_2 \end{bmatrix} \tag{8}$$

$$\frac{dv_{dc}}{dt} = \frac{3m_1}{4C_{dc}} \left[\cos\delta_1 \quad \sin\delta_1 \right] \begin{bmatrix} i_{1d} \\ i_{1q} \end{bmatrix} + \frac{3m_2}{4C_{dc}} \left[\cos\delta_2 \quad \sin\delta_2 \right] \begin{bmatrix} i_{2d} \\ i_{2q} \end{bmatrix} \tag{9}$$

where $x_{t1} = \omega l_1$, $x_{t2} = \omega l_2$ are the reactances of the series transformers.

3 System Model

3.1 Non Linear Model

Fig. 3 shows a Single machine infinite bus (SMIB) power system equipped with an IPFC. The system consists of a generator which is connected to the infinite bus through the two parallel transmission lines. An elementary IPFC consisting of two three-phase GTO based VSCs, each compensating a different transmission line by series voltage injection is installed on the two transmission lines.

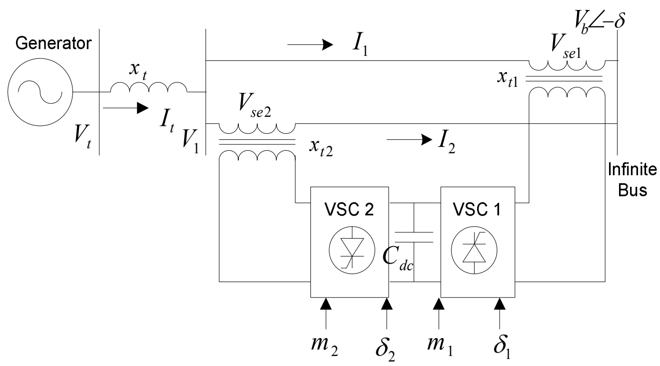

Fig. 3. An IPFC installed in a single machine infinite bus system

The VSCs are linked together at their DC terminals facilitating real power transfer among the transmission lines. The nonlinear dynamic model of the power system of Fig. 3 is derived as follows:

$$\dot{\delta} = \omega_0(\omega - 1) \tag{10}$$

$$\dot{\omega} = \frac{P_m - P_e - P_D}{M} \tag{11}$$

$$\dot{E}'_q = \frac{(-E_q + E_{fd})}{T'_{do}} \tag{12}$$

$$\dot{E}_{fd} = \frac{-E_{fd} + K_a(V_{ref} - V_t)}{T_a} \tag{13}$$

$$\begin{aligned}\dot{v}_{dc} &= \frac{3m_1}{4C_{dc}}(i_{1d}\cos\delta_1 + i_{1q}\sin\delta_1)\\ &\quad + \frac{3m_2}{4C_{dc}}(i_{2d}\cos\delta_2 + i_{2q}\sin\delta_2)\end{aligned} \tag{14}$$

where

$$P_e = P_1 + P_2 = v_{dt}i_{dt} + v_{qt}i_{qt}$$
$$E_q = E'_q + (x_d - x'_d)i_{dt} = E'_q + (x_d - x'_d)(i_{1d} + i_{2d})$$
$$v_{qt} = E'_q - x'_d\, i_{dt} = E'_q - x'_d\,(i_{1d} + i_{2d})$$
$$v_{dt} = x_q\, i_{qt} = x_q\,(i_{1q} + i_{2q})$$
$$v_t = \left(v_{dt}^2 + v_{qt}^2\right)^{1/2},$$
$$i_t = i_{dt} + ji_{qt},\ i_t = i_1 + i_2$$
$$i_{dt} = i_{1d} + i_{2d},\ i_{qt} = i_{1q} + i_{2q}$$

P_1, P_2 are the power flow in each of the transmission lines and δ, is the rotor angle of synchronous generator in radians, ω is rotor speed in rad/sec, V_t is the terminal voltage of the generator, $\dot{E}'_q$ is generator internal voltage, E_{fd} is the generator field voltage, v_{dc} is the voltage at DC link. I_1 and I_2 are the line currents flowing the transmission lines.

From the Fig. 3, we obtain:

$$V_t = jx_tI_t + V_1 \tag{15}$$

$$\begin{aligned}V_1 &= V_{set1} + jx_{L1}I_1 + V_b\\ &= V_{set2} + jx_{L2}I_2 + V_b\end{aligned} \tag{16}$$

where x_{L1}, x_{L2} are the transmission line reactances, therefore,

$$V_t = jx_tI_t + V_{set1} + jx_{L2}I_2 + V_b$$

$$\begin{aligned}v_{dt} + jv_{qt} &= x_q(i_{1q} + i_{2q}) + jE'_q - jx'_d(i_{1d} + i_{2d})\\ &= jx_t(i_{1d} + i_{2d} + ji_{1q} + ji_{2q}) + v_{se2td}\\ &\quad + j\,v_{se2tq} + j(x_{L2})(i_{2d} + ji_{2q})\\ &\quad + V_b\sin\delta + jV_b\cos\delta\end{aligned} \tag{17}$$

Solving the equations we get:

$$\begin{aligned}i_{1d} &= x_{11d}E'_q + \frac{1}{2}(x_{12d} - x_{11d})v_{dc}m_2\sin\delta_2\\ &\quad - \frac{1}{2}x_{12d}v_{dc}m_1\sin\delta_1 - x_{11d}v_b\cos\delta\end{aligned} \tag{18}$$

$$\begin{aligned}i_{2d} &= x_{21d}E'_q + \frac{1}{2}(x_{22d} - x_{21d})v_{dc}m_2\sin\delta_2\\ &\quad - \frac{1}{2}x_{22d}v_{dc}m_1\sin\delta_1 - x_{21d}v_b\cos\delta\end{aligned} \tag{19}$$

$$\begin{aligned}i_{1q} &= \frac{1}{2}(x_{11q} + x_{12q})v_{dc}m_2\cos\delta_2\\ &\quad - \frac{1}{2}(x_{12q})v_{dc}m_1\cos\delta_1 + x_{11q}v_b\sin\delta\end{aligned} \tag{20}$$

$$\begin{aligned}i_{2q} &= \frac{1}{2}(x_{21q} + x_{22q})v_{dc}m_2\cos\delta_2\\ &\quad - \frac{1}{2}(x_{22q})v_{dc}m_1\cos\delta_1 + x_{21q}v_b\sin\delta\end{aligned} \tag{21}$$

where

$$x_{11d} = x_{tL2}/x_{\Sigma1},\ x_{12d} = (x'_{dt} + x_{tL2})/x_{\Sigma1}$$

$$x_{21d} = x_{tL1}/x_{\Sigma1},\ x_{22d} = -x'_{dt}/x_{\Sigma1}$$

$$x_{11q} = x_{tL2}/x_{\Sigma2},\ x_{12q} = -(x'_{qt} + x_{tL2})/x_{\Sigma2}$$

$$x_{21q} = x_{tL1}/x_{\Sigma2},\ x_{22d} = -x'_{qt}/x_{\Sigma2}$$

$$x_{tL2} = x_{t2} + x_{L2}, x'_{dt} = x'_d + x_t$$

$$x_{tL1} = x_{t1} + x_{L1}, x'_{qt} = x_q + x_t$$

$$x_{\Sigma 1} = (x'_{dt}.x_{tL2}) + (x'_{dt} + x_{tL2})(x_{tL1})$$

$$x_{\Sigma 2} = (x'_{qt}.x_{tL2}) + (x'_{qt} + x_{tL2})(x_{tL1})$$

3.2 Linearized model

The linear Heffron-Phillips model of SMIB system installed with IPFC is obtained by linearizing the non linear model equations (10-21) which is obtained as follows:

$$\Delta\dot{\delta} = \omega_o \Delta\omega \tag{22}$$

$$\Delta\dot{\omega} = \frac{(\Delta P_m - \Delta P_e - D\Delta\omega)}{M} \tag{23}$$

$$\Delta\dot{E}'_q = \frac{-\Delta E_q + \Delta E_{fd}}{T'_{do}} \tag{24}$$

$$\Delta\dot{E}_{fd} = \frac{-\Delta E_{fd} + K_a(\Delta V_{ref} - \Delta V_t)}{T_a} \tag{25}$$

$$\Delta\dot{v}_{dc} = K_7\,\Delta\delta + K_8\,\Delta E'_q - K_9\,\Delta v_{dc} + K_{cm1}\,\Delta m_1 + K_{c\delta 1}\,\Delta\delta_1 + K_{cm2}\,\Delta m_2 + K_{c\delta 2}\,\Delta\delta_2 \tag{26}$$

where

$$\Delta P_e = K_1\,\Delta\delta + K_2\,\Delta E'_q + K_{pv}\,\Delta v_{dc} + K_{pm1}\,\Delta m_1 + K_{p\delta 1}\,\Delta\delta_1 + K_{pm2}\,\Delta m_2 + K_{p\delta 2}\,\Delta\delta_2 \tag{27}$$

$$\Delta E_q = K_4\,\Delta\delta + K_3\,\Delta E'_q + K_{qv}\,\Delta v_{dc} + K_{qm1}\,\Delta m_1 + K_{q\delta 1}\,\Delta\delta_1 + K_{qm2}\,\Delta m_2 + K_{q\delta 2}\,\Delta\delta_2 \tag{28}$$

$$\Delta V_t = K_5\,\Delta\delta + K_6\,\Delta E'_q + K_{vv}\,\Delta v_{dc} + K_{vm1}\,\Delta m_1 + K_{v\delta 1}\,\Delta\delta_1 + K_{vm2}\,\Delta m_2 + K_{v\delta 2}\,\Delta\delta_2 \tag{29}$$

The model has 28 K-constants which are functions of system parameters and the initial operating condition.

3.3 State Space Model

The power system is represented in state space as:

$$\dot{X} = AX + BU \tag{30}$$

where the state vector and control vector are:

$$X = [\Delta\delta \quad \Delta\omega \quad \Delta E'_q \quad \Delta E_{fd} \quad \Delta v_{dc}]^T$$

$$U = [\Delta m_1 \quad \Delta\delta_1 \quad \Delta m_2 \quad \Delta\delta_2]^T \tag{31}$$

and, state and control matrix are:

$$A = \begin{bmatrix} 0 & \omega_o & 0 & 0 & 0 \\ -\frac{K_1}{M} & -\frac{D}{M} & -\frac{K_2}{M} & 0 & -\frac{K_{pv}}{M} \\ -\frac{K_4}{T'_{do}} & 0 & -\frac{K_3}{T'_{do}} & \frac{1}{T'_{do}} & -\frac{K_{qv}}{T'_{do}} \\ -\frac{K_a K_5}{T_a} & 0 & -\frac{K_a K_6}{T_a} & -\frac{1}{T_a} & -\frac{K_a K_{vv}}{T_a} \\ K_7 & 0 & K_8 & 0 & -K_9 \end{bmatrix}$$

$$B = \begin{bmatrix} 0 & 0 & 0 & 0 \\ -\frac{K_{pm1}}{M} & -\frac{K_{p\delta 1}}{M} & -\frac{K_{pm2}}{M} & -\frac{K_{p\delta 2}}{M} \\ -\frac{K_{qm1}}{T'_{do}} & -\frac{K_{q\delta 1}}{T'_{do}} & -\frac{K_{qm2}}{T'_{do}} & -\frac{K_{q\delta 2}}{T'_{do}} \\ -\frac{K_a K_{vm1}}{T_a} & -\frac{K_a K_{v\delta 1}}{T_a} & -\frac{K_a K_{vm2}}{T_a} & -\frac{K_a K_{v\delta 2}}{T_a} \\ K_{cm1} & K_{c\delta 1} & K_{cm2} & K_{c\delta 2} \end{bmatrix}$$

and Δm_1 is the deviation in pulse width modulation index m_1 of voltage series converter 1 in line 1. Δm_2 is the deviation in pulse width modulation index m_2 of voltage series converter 2 in line 2. $\Delta\delta_1$ is the deviation in phase angle of the injected voltage V_{se1}. $\Delta\delta_2$ is the deviation in phase angle of the injected voltage V_{se2}.

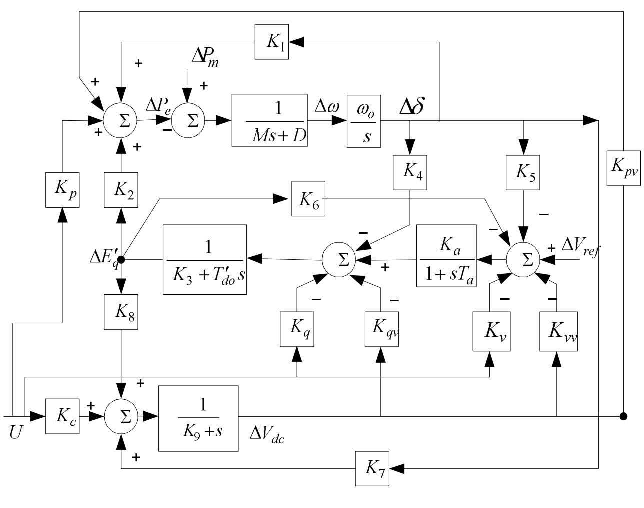

Fig. 4. Phillips-Heffron model of SMIB system installed with IPFC

The extended Phillips-Heffron model of SMIB system installed with IPFC (30) is shown as a block diagram in Fig. 4. It should be noted that K_p, K_q, K_v and K_c in Fig. 4 are the row vectors defined as

$$K_p = [K_{pm1} \quad K_{p\delta 1} \quad K_{pm2} \quad K_{p\delta 2}\ ]$$
$$K_q = [K_{qm1} \quad K_{q\delta 1} \quad K_{qm2} \quad K_{q\delta 2}\ ]$$
$$K_v = [K_{vm1} \quad K_{v\delta 1} \quad K_{vm2} \quad K_{v\delta 2}\ ]$$
$$K_c = [K_{cm1} \quad K_{c\delta 1} \quad K_{cm2} \quad K_{c\delta 2}\ ]$$

From (31), we observe that any of the four inputs control signals Δm_1, $\Delta\delta_1$, Δm_2 and $\Delta\delta_2$ can be utilized to superimpose on the damping function of IPFC.

4 IPFC Damping Controller

The damping controller is designed to contribute a positive damping torque in phase with the speed deviation to the electromechanical oscillation loop of the generator. The structure of the IPFC based damping controller is shown in Fig. 5, which comprises of gain K_{dc}, signal washout block and 'n' lead lag compensator blocks.

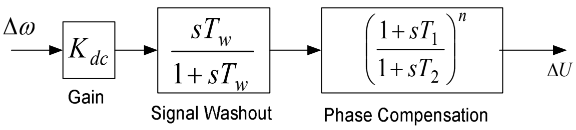

Fig. 5. Structure of IPFC based damping controller

The time constants of lead lag compensator are determined using the phase compensation method [21] to compensate the phase shift between the control input signal ΔU and electrical power deviation ΔP_e. The gain setting K_{dc} of the damping controller is chosen to achieve a required damping ratio of the electromechanical mode and the value of T_w (the washout filter time constant) is chosen in the range of 10 to 20s. The four control parameters, m_1, m_2, δ_1 and δ_2 can be modulated to produce the damping torque. The damping controller based on the IPFC input signal m_1 is termed as the damping controller m_1 and consequently other controller based on input signals m_2, δ_1 and δ_2 are termed as damping controller m_2, damping controller δ_1 and damping controller δ_2.

5 Simulation Results

A single machine infinite bus power system installed with IPFC is considered for analysis, parameters of which are given in Appendix A. The system is operated with various different load conditions, i.e., from $P_e = 0.1$ pu to $P_e = 1.5$ pu, and $V_t = 1.02$ pu, $V_b = 1.0$ pu. The linearized model is obtained at each varying condition and eigenvalue analysis is performed. The values of the K constants of the system at the one operating point P_e = 0.8 pu is given in the Appendix B. Eigenvalues for the power system at this operating point are shown in Table 1. The system contains a pair of complex eigenvalues having low damping ratio of 0.0084952. A controller is designed to tune the gain K_{dc} to achieve a damping ratio of 0.1. The various damping controllers are designed at the operating point P_e = 0.8 pu, where the parameters of each controller is given in the Appendix C.

Table 1: Eigenvalues of the linearized SMIB at operating point P_e = 0.8 pu.

Eigenvalues	Damping Ratio	Frequency
-100.09	1	0
-0.09782 ± j11.514	0.0084952	1.8325
-0.31442	1	0
-0.0023063	1	0

The dynamic performance of the system is examined using the alternative damping controllers with varying operating conditions. The responses are shown for the operating conditions P_e = 0.8 pu the nominal condition, P_e = 0.2 pu light load condition and P_e = 1.4 pu the heavy load condition.

5.1 Operating point P_e = 0.8 pu

The effectiveness of IPFC damping controllers at the nominal operating condition P_e = 0.8 pu at which they are designed is observed. The power system performance in the presence of the controllers is investigated with the non linear simulation of the system modelled by the nonlinear differential equations (10-21). A three phase fault occurs at 1.0 sec at the starting end of the transmission line and cleared after 100 ms. The response of the system without the controller (marked by 'no controller') is shown with dotted line and the responses with IPFC controller is shown with solid line marked by the arrow "with controller".

5.1.1 Damping Controller m_1

The system eigenvalues in the presence of the damping controller m_1 is shown in Table 2.

Table 2: Eigenvalues of the linearized SMIB at operating point $P_e = 0.8$ pu with damping controller m_1

Eigenvalues	Damping Ratio	Frequency
0	-	0
-100.01	1	0
-1.2986 ± j11.531	0.11191	1.8353
-6.5463	1	0
-0.37662	1	0
-0.095395	1	0
-0.0023062	1	0

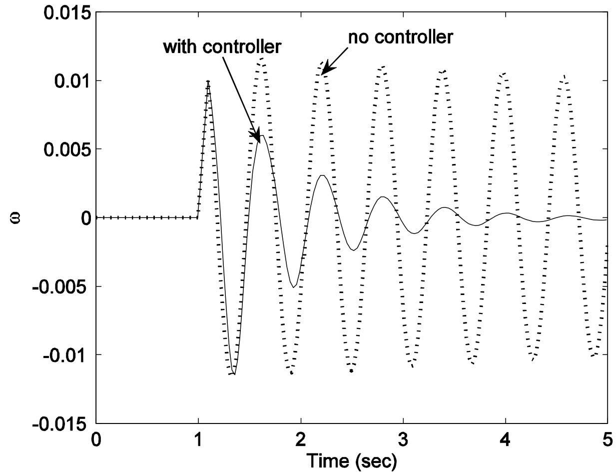

Fig.6. Rotor Speed response with and without damping controller m_1 at $P_e = 0.8$ pu

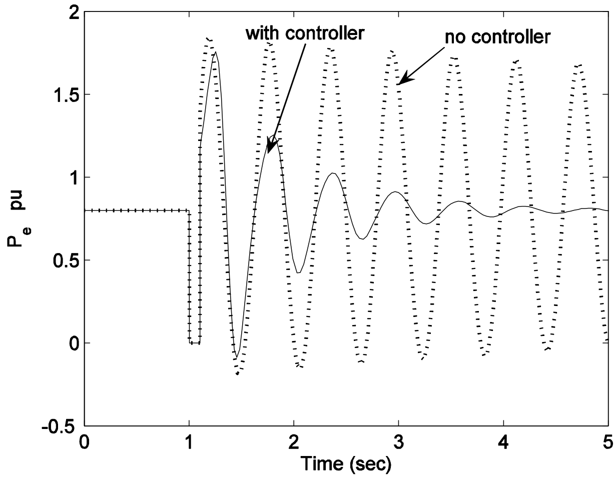

Fig. 7. Electrical Power response with and without damping controller m_1 at $P_e = 0.8$ pu.

The complex eigenvalue pair's damping ratio has increased to approximately 0.11 as desired. The rotor speed and electrical power response during and after the fault clearance, with and without the controller is shown in Fig. 6 and Fig. 7 respectively. It is clear from these Figures that, the system is oscillating without the controller due to the poor damping of the oscillation modes and as such power system oscillations are clearly observed. It is also seen, that the use of the proposed IPFC damping controller m_1 the oscillations are suppressed in about 4.5 sec. after the fault is cleared i.e at 5.5sec, simulation time.

5.1.2 Damping Controller m_2

Table 3 gives the eigenvalues of the system in the presence of the damping controller m_2. The damping ratio of the pair of complex eigenvalues has increased to 0.10877 with the use of this

Table 3: Eigenvalues of the linearized SMIB at operating point $P_e = 0.8$ pu with damping controller m_2

Eigenvalues	Damping Ratio	Frequency
0	-	0
-100.08	1	0
-1.2541 ± j11.461	0.10877	1.8241
-11.003	1	0
-0.0023052	1	0
-0.1	1	0
-0.31631	1	0

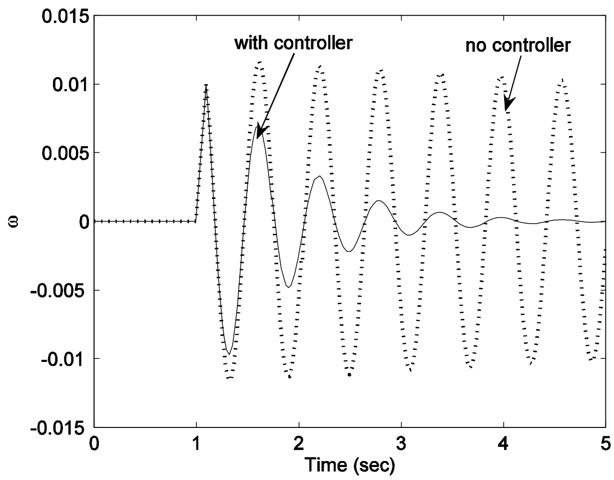

Fig. 8. Rotor Speed response with and without damping controller m_2 at $P_e = 0.8$ pu

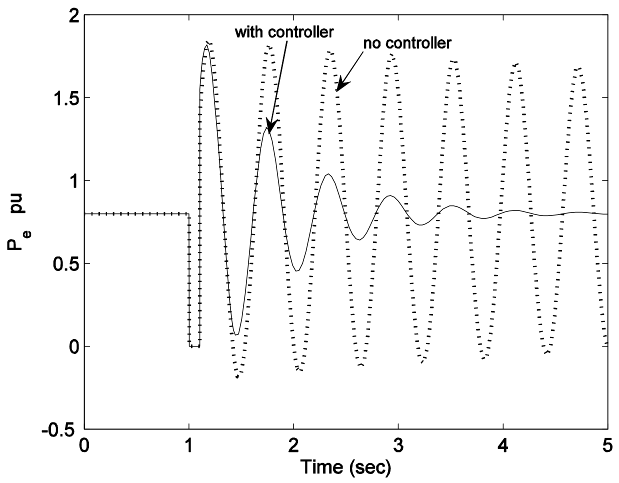

Fig. 9. Electrical Power response with and without damping controller m_2 at $P_e = 0.8$ pu

damping controller at the operating point $P_e = 0.8$ pu as per the designed requirement. Fig. 8 and Fig. 9 show the rotor speed and electrical power response in the presence of the damping controller m_2 from the nonlinear simulation. The oscillations occurring due to the fault are mitigated at the time of 4.5 sec i.e around 3.5 sec after the fault clearance. The controller m_2 is comparatively better than the damping controller m_1 and also, in the value of the gain K_{dc} required by the controllers to achieve same performance. The gain of the controller m_1 is much higher (equal to 182.12) compared to the gain of the damping controller m_2 which is equal to 15.235. As such the damping controller m_2 is much more effective than damping controller m_1.

5.1.3 Damping Controller δ_1

The eigenvalues of the system with the damping controller δ_1 is given in the Table 4. The controller achieves the damping ratio of 0.10189 for the pair of

Table 4: Eigenvalues of the linearized SMIB at operating point $P_e = 0.8$ pu with damping controller δ_1

Eigenvalues	Damping Ratio	Frequency
0	-	0
-22.599 ± j94.966	0.23151	15.114
-105.84	1	0
-1.139 ± j11.12	0.10189	1.7698
-0.31395	1	0
-0.10005	1	0
-0.0023063	1	0

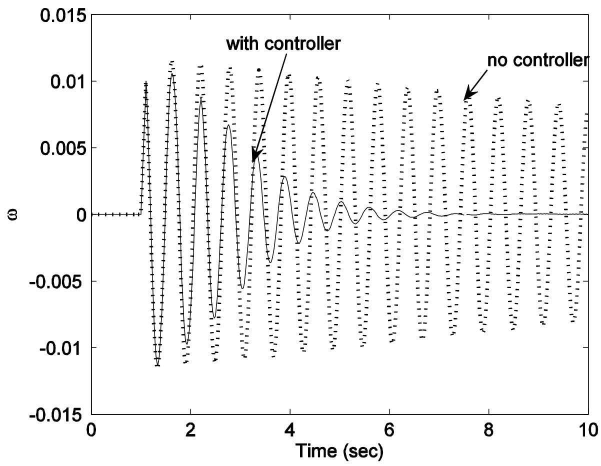

Fig. 10. Rotor Speed response with and without damping controller δ_1 at $P_e = 0.8$ pu

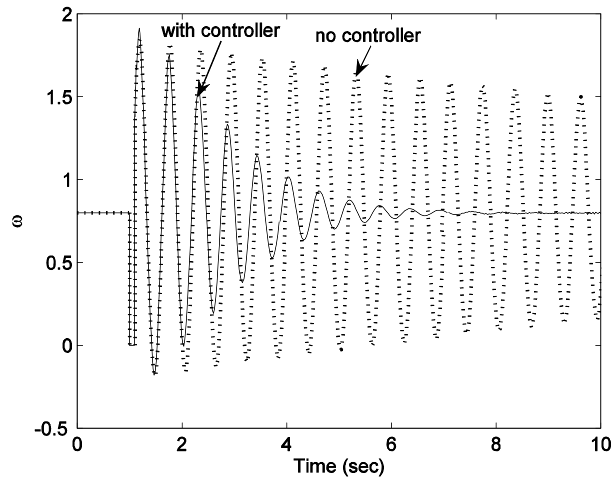

Fig. 11. Electrical Power response with and without damping controller δ_1 at $P_e = 0.8$ pu

complex eigenvalues and phase is compensated by two lead lag compensator blocks (n = 2) as compared to controllers m_1 and m_2 which require only one lead lag block. The rotor speed response ω and electrical power P_e is shown in Fig. 10 and Fig. 11 respectively. It is observed from the responses that the oscillations are sustained around 7.5 sec. The damping controller δ_1 is less effective compared to the other two controllers m_1 and m_2 as it requires more time to dampen the oscillations.

5.1.4 Damping Controller δ_2

Table 5 shows the eigenvalues of the system with the damping controller δ_2. However, this controller does not contribute much to the damping of the oscillation mode as seen from the eigenvalues, damping ratio in Table 5, although the gain of the damping controller is significantly large.

Table 5: Eigenvalues of the linearized SMIB at operating point $P_e = 0.8$ pu with damping controller δ_2

Eigenvalues	Damping Ratio	Frequency
0	-	0
-100.09	1	0
-0.15569 ± j10.191	0.015275	1.622
-0.1734 ± j0.21481	0.62812	0.034188
-0.10615	1	0
-0.05592	1	0
-0.0023054	1	0

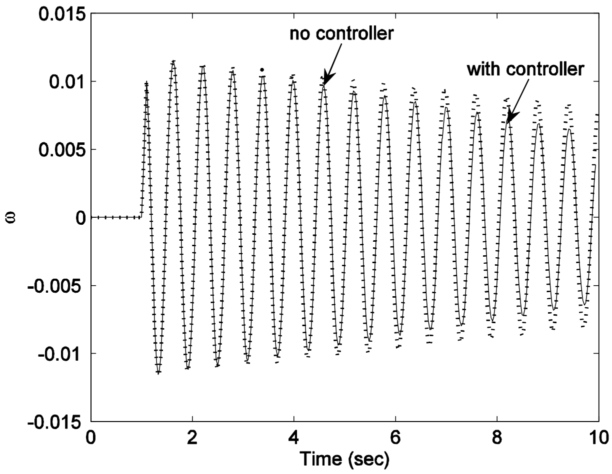

Fig. 12. Rotor Speed response with and without damping controller δ_2 at $P_e = 0.8$ pu

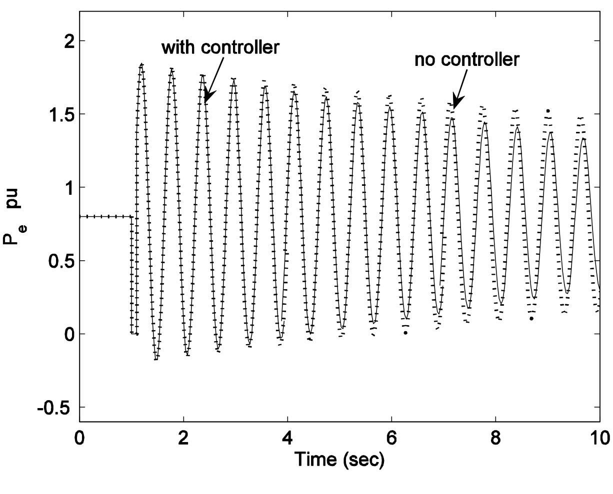

Fig. 13. Electrical Power response with and without damping controller δ_2 at $P_e = 0.8$ pu

Further increase of the gain of the controller only pushes the system to instability as the eigenvalues are forced into the RHS of the S plane. The responses of the rotor speed and electrical power of the system with the damping controller δ_2 is shown in Fig. 12 and Fig. 13 respectively. It is seen that the effect of the controller on the oscillations is negligible and inferior compared to the other three controllers.

5.2 Operating point P_e = 0.2 pu (light load condition)

The performance of the controllers at different load condition, i.e, at a lighter load condition $P_e = 0.2$ pu is examined other than the operating point whether the controllers have been designed.

5.2.1 Damping Controller m_1

The eigenvalues of the power system at $P_e = 0.2$ pu with the damping controller m_1 is given in Table 6.

Table 6: Eigenvalues of the linearized SMIB at operating point $P_e = 0.2$ pu with damping controller m_1

Eigenvalues	Damping Ratio	Frequency
0	-	0
-100.18	1	0
-8.7464 ± j15.604	0.48895	2.4835
-3.4176	1	0
-0.00077924	1	0
-0.10315	1	0
-0.34957	1	0

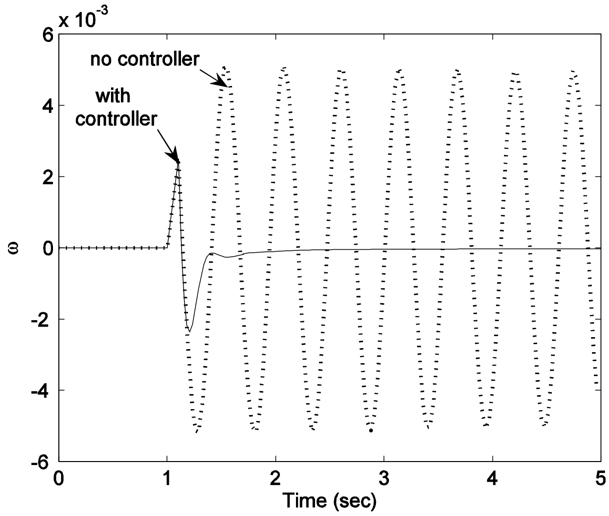

Fig. 14. Rotor Speed response with and without damping controller m_1 at $P_e = 0.2$ pu.

The damping controller is very effective at lighter load condition as it increases the damping ratio to a higher value of 0.48895 as seen from Table 6. Fig. 14 and Fig. 15 show the rotor speed and electrical power response with and with out the damping controller at P_e = 0.2 pu. The damping controller m_1 is able to sustain the oscillations at a faster rate approximately within 1.0 sec. after the fault occurrence as compared to Fig. 6 and Fig., where the settling time is 4.5 sec. It is thus observed that the damping controller m_1 contributes more damping for lighter load conditions.

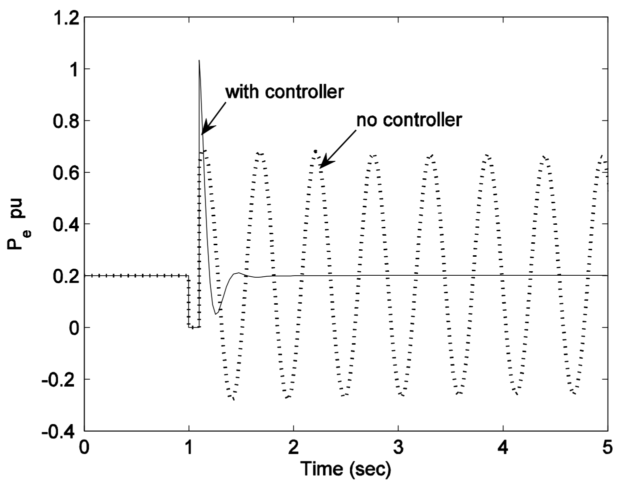

Fig. 15. Electrical Power response with and without damping controller m_1 at P_e = 0.2 pu

5.2.2 Damping Controller m_2

Table 7 shows the eigenvalues of the system with the damping controller m_2 at the operating point P_e = 0.2 pu. The damping controller increases the damping of the oscillation mode slightly at lighter load condition. This is also observed in the response of the rotor speed and electrical power in Fig. 16 and Fig. 17 respectively. The damping of the oscillation is at 3.5 sec, improving by one sec when compared to Fig 8 and Fig. 9 at the operating point of P_e = 0.8 pu .

Table 7: Eigenvalues of the linearized SMIB at operating point P_e = 0.2 pu with damping controller m_2

Eigenvalues	Damping Ratio	Frequency
0	-	0
-100.19	1	0
-1.4903 ± j12.232	0.12094	1.9468
-10.987	1	0
-0.00077932	1	0
-0.10031	1	0
-0.34438	1	0

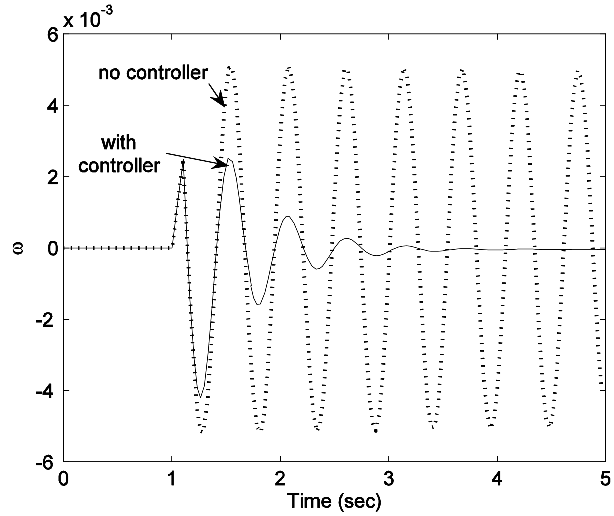

Fig. 16. Rotor Speed response with and without damping controller m_2 at P_e = 0.2 pu.

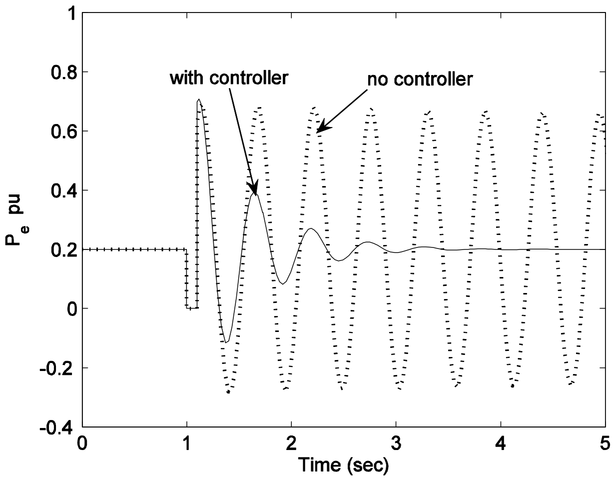

Fig. 17. Electrical Power response with and without damping controller m_2 at P_e = 0.2 pu

5.2.3 Damping Controller δ_1

The eigenvalues of the power system with the damping controller δ_1 is given in Table 8. The damping contributed by this controller is less as compared to damping controllers m_1 and m_2 at this operating point. The damping ratio of the oscillation mode is only 0.034505 which is very less than the required 0.1 value. Fig. 18 and Fig. 19 show the response of the rotor speed and electrical power

Table 8: Eigenvalues of the linearized SMIB at operating point P_e = 0.2 pu with damping controller δ_1.

Eigenvalues	Damping Ratio	Frequency
0	-	0
-71.472 ± j64.643	0.74165	10.288
-100.81	1	0
-0.42678 ± j12.361	0.034505	1.9673
-0.34466	1	0
-0.1	1	0
-0.00077932	1	0

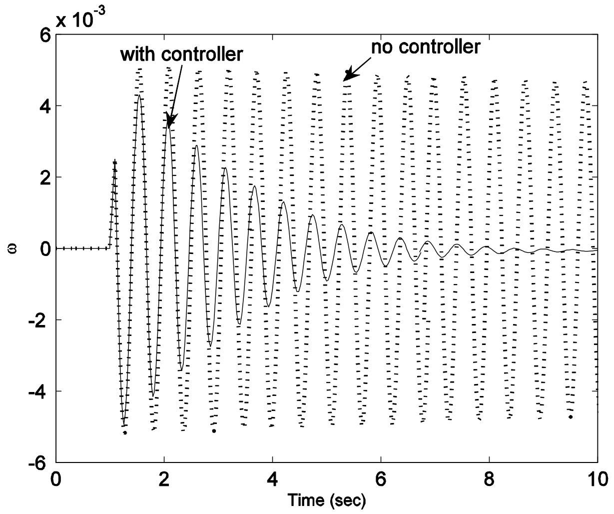

Fig. 18. Rotor Speed response with and without damping controller δ_1 at P_e = 0.2 pu.

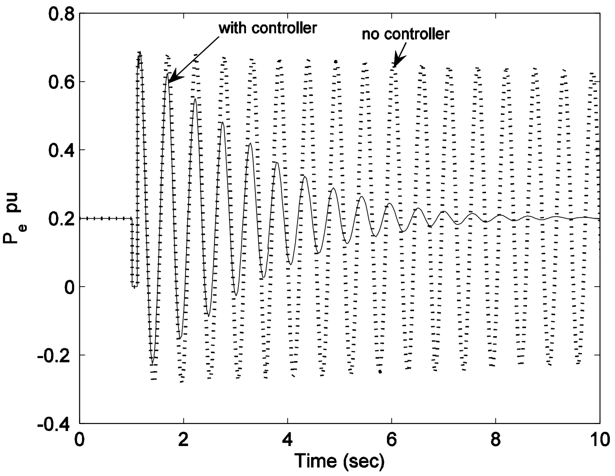

Fig. 19. Electrical Power response with and without damping controller δ_1 at P_e = 0.2 pu

respectively in the presence of the damping controller δ_1. The settling time is around 9.5 sec which is more compared to the settling times when the damping controllers m_1 and m_2 are used at the two different operating points P_e = 0.2 pu and P_e = 0.8 pu.

5.2.4 Damping Controller δ_2

Table 9 gives the eigenvalues when the damping controller δ_2 is placed in the power system. As observed during the operating point P_e = 0.8 pu, this controller also does not contribute to any damping during the operating point P_e = 0.2 pu as seen in Table 9. This is also verified from the responses of rotor speed and electrical power in Fig. 20 and Fig. 21 respectively. The controller does not help in mitigating the power system oscillations. Thus damping controller δ_2 is not suitable for improving the damping of the oscillation mode.

Table 9: Eigenvalues of the linearized SMIB at operating point P_e = 0.2 pu with damping controller δ_2

Eigenvalues	Damping Ratio	Frequency
0	-	0
-100.2	1	0
-0.027141± j11.736	0.0023127	1.8678
-0.00078018	1	0
-0.062618	1	0
-0.10615	1	0
-0.24777 ± j0.049733	0.98044	0.0079153

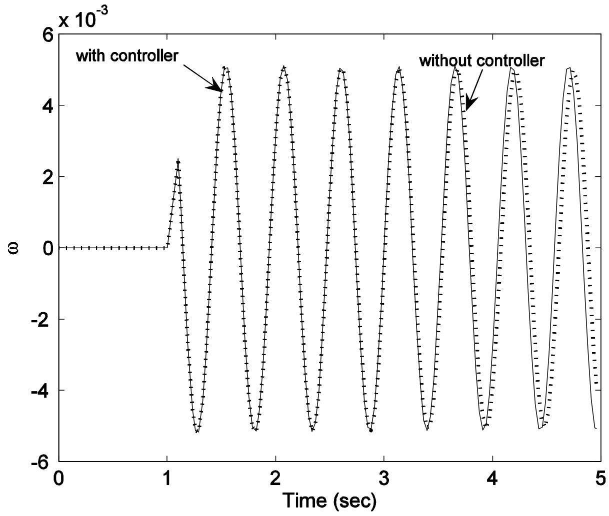

Fig. 20. Rotor Speed response with and without damping controller δ_2 at P_e = 0.2 pu.

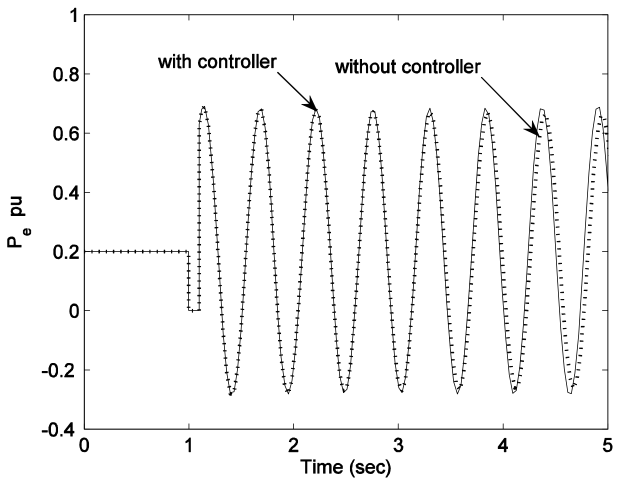

Fig. 21. Electrical Power response with and without damping controller δ_2 at $P_e = 0.2$ pu

5.3 Operating point P_e = 1.4 pu (heavy load condition)

The damping controller performance of the power system is observed for the operating point $P_e = 1.4$ pu i.e at heavy load condition with various damping controllers.

5.3.1 Damping Controller m_1

The eigenvalues of the power system at $P_e = 1.4$ pu with the damping controller m_1 is given in Table 10. It appears that the damping controller m_1 contributes negative damping at heavy load conditions as observed from Table 10. The oscillation mode is forced into the RHS of the S - plane. But upon the non linear simulation of the system with this controller m_1, we observe a peculiarity in the responses of the rotor speed and electrical power as shown in Fig. 22 and Fig. 23

Table 10: Eigenvalues of the linearized SMIB at operating point $P_e = 1.4$ pu with damping controller m_1

Eigenvalues	Damping Ratio	Frequency
0	-	0
-100.19	1	0
2.6187 ± j9.2251	-0.27308	1.4682
-8.79	1	0
-0.81499	1	0
-0.097471	1	0
6.4304e-005	-1	0

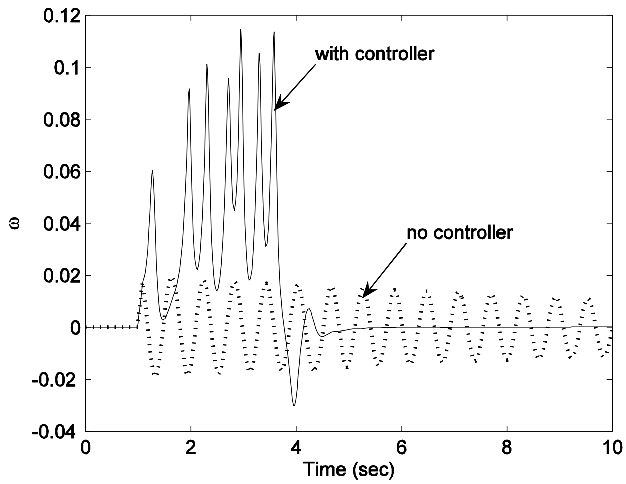

Fig. 22. Rotor Speed response with and without damping controller m_1 at $P_e = 1.4$ pu.

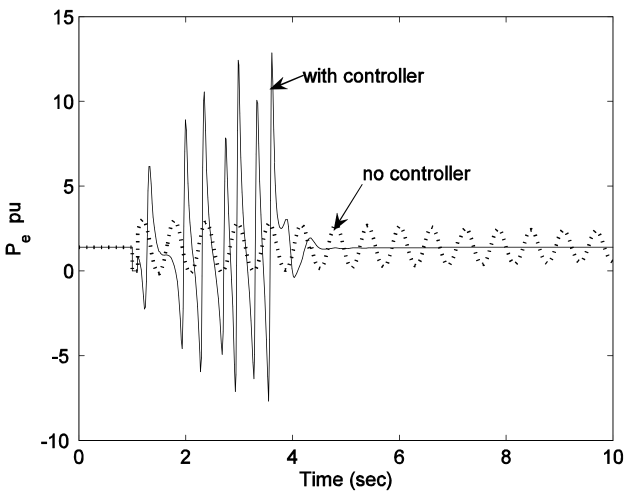

Fig. 23. Electrical Power response with and without damping controller m_1 at $P_e = 1.4$ pu.

respectively. The oscillation seems to increase in amplitude with high peak overshoots as if leading the system to instability reflecting the eigenvalues computed in Table 10. But at time 4.5 sec the oscillation suddenly are mitigated. This unusual nature of the damping controller m_1 providing excessive damping at light load condition, providing damping at heavy load condition with high peak values and requirement of higher gain value to provide the required damping makes it unreliable for damping the power system oscillations consistently for all operating conditions.

5.3.2 Damping Controller m_2

Table 11 represents the eigenvalues of the power system with the damping controller m_2. At heavy load condition the controller provides a damping about 5.7%. The oscillations in the rotor speed and

Table 11: Eigenvalues of the linearized SMIB at operating point $P_e = 1.4$ pu with damping controller m_2

Eigenvalues	Damping Ratio	Frequency
0	-	0
-99.847	1	0
-0.6271 ± j10.91	0.057388	1.7363
-11.039	1	0
-0.71301	1	0
-0.099809	1	0
6.4304e-005	-1	0

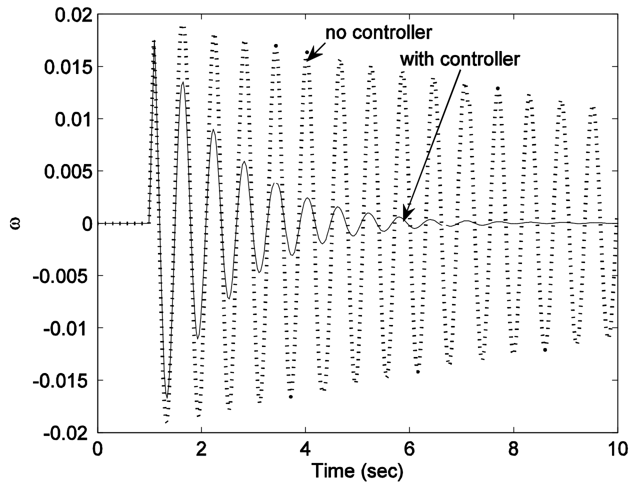

Fig. 24. Rotor Speed response with and without damping controller m_2 at $P_e = 1.4$ pu.

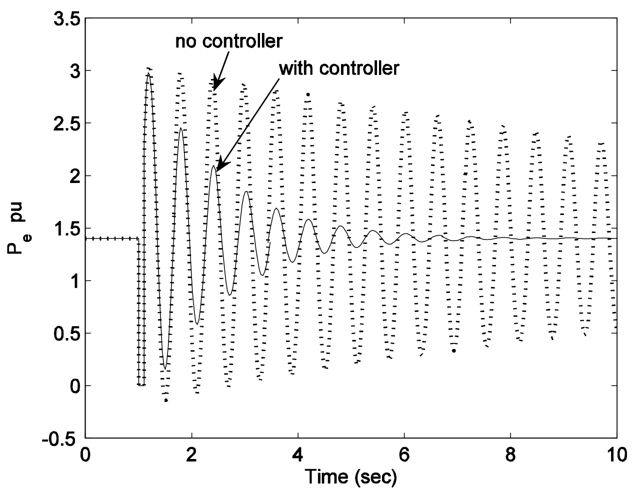

Fig. 25. Electrical Power response with and without damping controller m_2 at $P_e = 1.4$ pu.

electrical power is shown in Fig. 24 and Fig. 25 respectively. The damping controller m_2 dampens the oscillations at about 7.5 sec for heavy load condition. This damping controller m_2 provides sufficient damping at lighter load condition $P_e = 0.2$ pu and nominal load condition $P_e = 0.8$ pu. However, its performance in heavy load condition $P_e = 1.4$ pu does not meet the designed requirement of achieving the damping ratio of 0.1 although it mitigates the oscillation consistently.

5.3.3 Damping Controller δ_1

The eigenvalues of the system with the damping controller δ_1 is shown in Table 12. The damping controller δ_1 contributes slightly to the oscillation mode of interest and it also introduces another set of

Table 12: Eigenvalues of the linearized SMIB at operating point $P_e = 1.4$ pu with damping controller δ_1

Eigenvalues	Damping Ratio	Frequency
0	-	0
-116.91	1	0
-27.566 ± j96.088i	0.27576	15.293
-0.87469± j9.8899	0.088099	1.574
-0.69493	1	0
-0.10006	1	0
6.4304e-005	-1	0

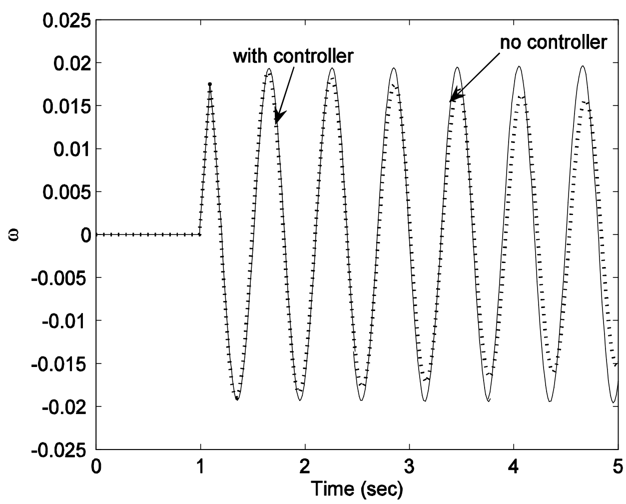

Fig. 26. Rotor Speed response with and without damping controller δ_1 at $P_e = 1.4$ pu.

complex eigenvalues, though it has sufficient damping ratio. However the responses obtained from the nonlinear simulation as shown in Fig. 26 and Fig. 27 for rotor speed and electrical power output respectively indicate the ineptness of this controller to provide damping compared to the other damping controllers m_1 and m_2. The responses indicate that the controller is ineffective in damping the oscillations at heavy load conditions.

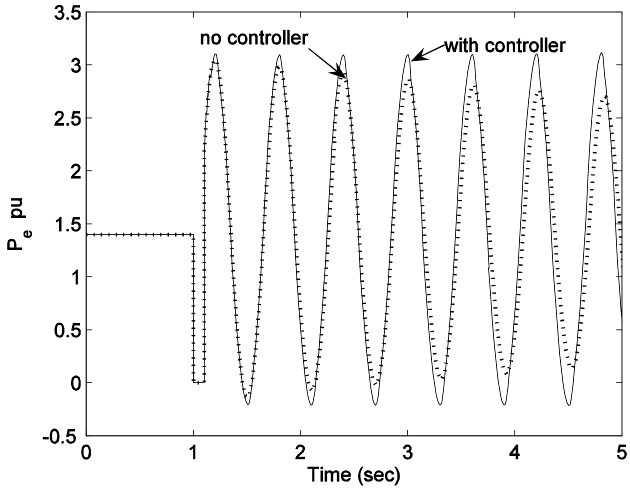

Fig. 27. Electrical Power response with and without damping controller δ_1 at P_e = 1.4 pu.

5.3.4 Damping Controller δ_2

The damping controller δ_2 is not a suitable signal for damping as can be observed from Table 13 where the eigenvalues of oscillation mode are shifted to RHS of S-plane making the system unstable. This is also seen in Fig 28 and 29 that the controller does not provide any damping.

Table 13: Eigenvalues of the linearized SMIB at operating point P_e = 1.4 pu with damping controller δ_2

Eigenvalues	Damping Ratio	Frequency
0	-	0
-99.873	1	0
0.02401 ± j9.9107	-0.0024226	1.5773
-0.75652	1	0
-0.14535	1	0
-0.10615	1	0
-0.083081	1	0
6.4306e-005	-1	0

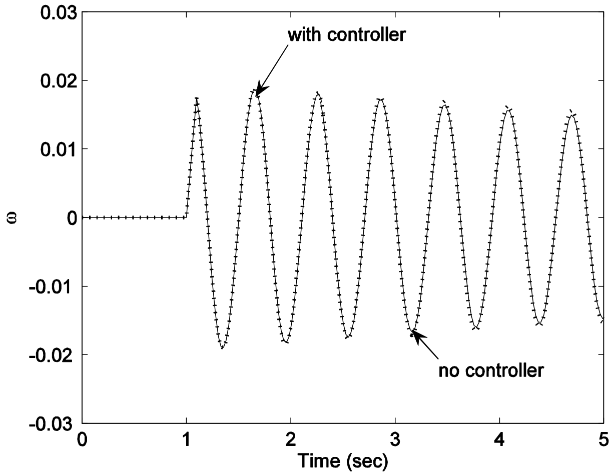

Fig. 28. Rotor Speed response with and without damping controller δ_2 at P_e = 1.4 pu.

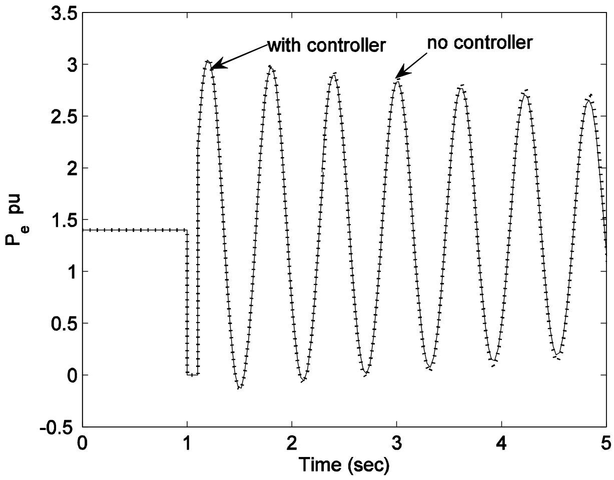

Fig. 29. Electrical Power response with and without damping controller δ_2 at P_e = 1.4 pu.

From the analysis we have deducted that the controller δ_2 is inept in providing damping to the power system oscillations. m_1 and m_2 prove to be suitable input signals on which the damping function can be added. However the damping controller m_2 is more efficient as the required damping is provided at minimum control cost, and it provides consistent damping throughout the varying operating conditions. This is also proved with the controllability index given in Table 14; from we can observe that the input signal m_2 is the most efficient signal for damping as it has higher value of controllability index compared to other input signals.

Table 14: Controllability indices with different IPFC controllable parameters

Input signal	Controllability index
m_1	0.0170
δ_1	0.0055
m_2	0.1560
δ_2	0.0079

Furthermore, if the operating condition where the IPFC damping controller is least effective is selected for the design of damping controller then it becomes more effective in damping at other operating conditions indicating its robustness. As we have seen, the damping controller m_2 is least effective at heavy load condition comparatively, and also the damping ratio of the concerned oscillation mode is the least at the operating condition of P_e = 1.4 pu as indicated in Table 15. Consequently the damping controller is designed at the operating point P_e = 1.4 pu and its performance at varying operating conditions is observed in Fig. 30. The results of the eigenanalysis with damping controller m_2, designed at the operating point P_e=1.4 pu, at different operating conditions are shown in Table 16. It is observed that the controller provides damping without sharp drops or increases in the damping contribution with various operating conditions

Table 15: Oscillation modes at various operating conditions

Op. Pt.	Eigenvalues without damping		
	Eigenvalues	Damping ratio	Frequ-ency
0.2	-0.031219 ± j12.275	0.0025433	1.9536
0.8	-0.09782 ± j11.514	0.0084952	1.8325
1.4	-0.016734 ± j11.009	0.00152	1.7521

Table 16: Oscillation modes at various operating conditions with damping controller m_2 designed at P_e=1.4 pu

Op. Pt.	Eigenvalues with damping m_2		
	Eigenvalues	Damping ratio	Frequ-ency
0.2	-2.6316 ± j12.503	0.20596	1.99
0.8	-2.1822 ± j11.669	0.18382	1.8573
1.4	-1.1397 ± j10.965	0.10338	1.7451

making the damping controller m_2 more robust and effective. Fig. 30 shows the rotor speed response with the damping controller m_2 at different load conditions. It is noted that the oscillations are mitigated at a faster rate with lighter load conditions which validates the results of Table 16.

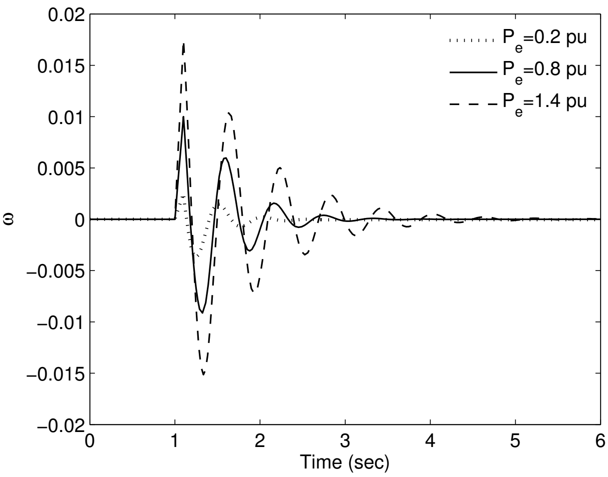

Fig. 30. Rotor Speed response with controller m_2 with varying operating conditions

The effect of the IPFC damping controller m_2 is also verified during a step variation of 0.01 pu in mechanical power input P_m. Fig. 31 shows the response of the electrical power when the disturbance is given at 1.0 sec. The effect of the damping controller m_2 designed at the two operating conditions P_e = 0.8 pu and at P_e = 1.4 pu is compared during this disturbance.

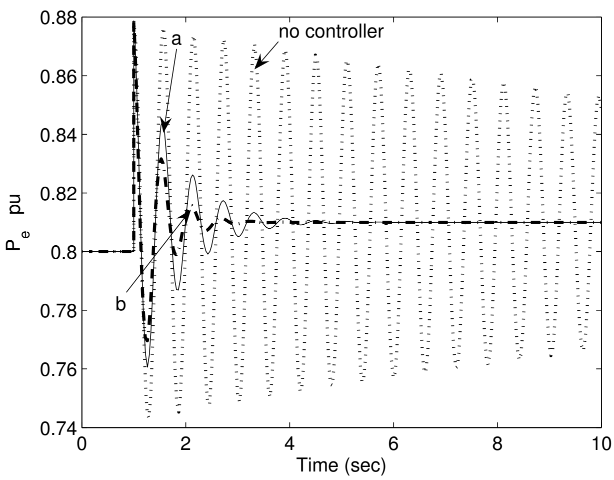

Fig. 31. Electrical Power response without damping controller and with damping controller m_2 designed at (a) P_e = 0.8 pu (b) P_e = 1.4 pu

It is clearly seen that the damping controller m_2 designed at the operating point P_e = 1.4 pu gives better damping as the settling time is at 3 sec. It improves the performance by 55% in comparison with the controller designed at P_e = 0.8 pu. Thus the controller is more robust when designed at the operating point at which the damping ratio of the oscillation mode is minimum or where it is least effective to ensure to effectiveness at other operating conditions. The operating point and the input signal play a significant role in damping the power system oscillations.

6 Conclusion

In this paper the non linear model of the IPFC has been developed and the extended linearized Phillips-Heffron model of a single machine infinite bus power system incorporated with IPFC is established. The parameters of the IPFC damping controller is determined using the phase compensation method based on the linearized model. The relative effectiveness of the input control signals Δm_1, $\Delta\delta_1$, Δm_2 and $\Delta\delta_2$ has been examined on example power system subjected to various disturbances. Investigations revealed that control signal Δm_2 is the most efficient of the input control signals to be used for damping in the power system whereas the control signal $\Delta\delta_2$ is inefficient in providing the damping. It is found that the IPFC damping controller is more robust over various operating conditions when the controller is designed at appropriate operating condition. The effectiveness and robustness of the IPFC damping controller is validated through eigenanalysis and non linear simulation. The authors are further investigating the additional damping provided by the proposed IPFC based damping controller in a multi-machine power system incorporated with IPFC.

References:

[1] F.P. DeMello and C. Concordia, Concepts of Synchronous Machine Stability as Affected by Excitation Control, *IEEE Transactions on Power Apparatus and Systems,* Vol. PAS-88, 1969, pp. 316-329.

[2] E.V. Larsen and D.A. Swann, Applying Power System Stabilizers, Parts I - 111, *IEEE Transactions on Power Apparatus and Systems,* Vol. PAS-100, 1981, pp. 3017-3046.

[3] J. H. Chow and J. J. Sanchez-Gasca, Pole-placement design of power System Stabilizers, IEEE T-PWRS, Vo1.4, 1989.

[4] R. Sadikovic, P. Korba and G. Andersson, Application of FACTS Devices for Damping of Power System Oscillations, *IEEE PowerTech* 2005, Russia, June 2005.

[5] P. K. Dash, S. Mishra, G. Panda, Damping Multimodal Power System Oscillation Using a Hybrid Fuzzy Controller for Series Connected FACTS Devices, *IEEE Transactions on Power Systems*, Vol. 15, No. 4, November 2000, pp. 1360 − 1366.

[6] H. F. Hang, Design of SSSC Damping Controller to Improve Power System Oscillation Stability, IEEE 1999.

[7] N. Tambey and M. L. Kothari, Damping of Power System Oscillation with Unified Power Flow Controller, *IEE Proc. Gener. Trans. Distib.* Vol. 150, No. 2, March 2003, pp. 129 – 140.

[8] A. Kazemi and F. Mahamnia, Improving of Transient Stability of Power Systems by Supplementary Controllers of UPFC using different Fault Conditions, *WSEAS Transaction on Power Systems*, Issue 7, Vol. 3, July 2008, pp. 547-556.

[9] S. N. Dhurvey and V. K. Chandrakar, Performance Comparison of UPFC in Coordination and Optimized POD and PSS on Damping of Power System Oscillations, *WSEAS Transaction on Power Systems*, Issue 5, Vol. 3, May 2008, pp. 287-299.

[10] N. G. Hingorami, L.Gyugyi, *Understanding FACTS: Concepts and Technology of Flexible AC Transmission system*, IEEE Press, 1999

[11] Y. H. Song and A. T. Johns, *Flexible AC Transmission systems*, IEE Power and Energy series 30, 1999.

[12] M. Ahmadzadeh, S. S. Mortazavi, A. Saeedian, A Novel Method of coordinating PSSs and FACTS Devices in Power System stability Enhancement, *WSEAS Transaction on Power Systems* Issue 5, Vol. 4, May 2009, pp. 177-188.

[13] L. Gyugyi, K. K. Sen, and C. D. Schauder, The interline power flow controller concept: A new approach to power flow management in transmission systems, *IEEE Trans. Power Del.*, Vol. 14, No. 3, Jul. 1999, pp. 1115–1123.

[14] X. Wei, J. H. Chow, B. Fardanesh, Ahdel-Aty Edris, A common modeling framework of voltage-sourced converters for loadflow, sensitivity, and dispatch analysis, *Power Engineering Society General Meeting*, IEEE Vol. 4, July 2003, pp. 13-17.

[15] J. Zhang, A. Yokoyama, A Comparison between the UPFC and the IPFC in Optimal

[16] Power Flow Control and Power Flow Regulation, *38th North American Power Symposium, NAPS 2006* , Sept. 2006, pp. 339–345.
[17] Wei, X.; Chow, J. H.; Fardanesh, B.; Edris, A.A, A dispatch strategy for an interline power flow controller operating at rated capacity, *Power Systems Conference and Exposition, IEEE PES*, 10-13 Oct. 2004, Vol.3, pp. 1459 - 1466.
[18] J. Chen, T. T. Lie, D. M. Vilathgamuwa, Basic control of interline power flow controller, *Power Engineering Society Winter Meeting*, IEEE Volume 1, 27-31 Jan. 2002, Vol.1, pp. 521 – 525.
[19] J. Chen, T. T. Lie, D. M. Vilathgamuwa, Design of an interline power flow controller, 14th PSCC, Sevilla, 24-28 June 2002.
[20] A. Kazemi, E. Karimi, The Effect of Interline Power Flow Controller (IPFC) on Damping Inter-area Oscillations in the Interconnected Power Systems, *Industrial Electronics, 2006 IEEE International Symposium*, Vol. 3, July 2006, pp. 1911 – 1915.
[21] A. Nabavi-Niaki, M. R. Iravani, Steady-state and dynamic models of unified power flow controller (UPFC) for power system studies, *IEEE Trans. Power Systems*, Vol. 11, No. 4, Nov. 1996, pp. 1937-1943.
[22] H. F. Wang, M. Li, and F. J. Swift, FACTS-based stabilizer designed by the phase compensation method. Part I and 11, *Proceedings of APSCOM-97*, Hong Kong, 1997, pp. 638-649.

Appendix

Appendix A

The parameters of the single machine infinite bus power system are as follows (in pu except where indicated):

$H = 4.0$s., $D = 0.0$, $T'_{d0} = 5.044$s.,
$x_d = 1.0$, $x_q = 0.6$, $x'_d = 0.3$,
$x_t = 0.01$, $x_{t1} = 0.015$, $x_{t2} = 0.015$,
$x_{L1} = 0.05$, $x_{L2} = 0.05$, $K_A = 10.0$,
$T_A = 0.01$s., $v_{dc0} = 225$KV, $P_{e0} = 0.8$,
$V_{b0} = 1.0$, $V_t = 1.02$.

Appendix B

K constants at the operating point of P_e=0.8 pu

K_1=3.166416, K_2=0.323807 K_3=3.043796
K_4=0.066681 K_5=-0.104002 K_6=-0.001198
K_7=0.002149 K_8=-0.009759 K_9=0.000035
K_{pv}=0.123469 K_{qv}=-0.004512 K_{vv}=0.012725
K_{pm1}=1.497362 $K_{p\delta1}$=-0.008114
K_{pm2}=1.578447 $K_{p\delta2}$=-0.017687
K_{qm1}=-0.285734 $K_{q\delta1}$=-0.015464
K_{qm2}=-0.031945 $K_{q\delta2}$=-0.144520
K_{vm1} =0.129343 $K_{v\delta1}$=0.000640
K_{vm2}=0.165458 $K_{v\delta2}$=0.028441
K_{cm1}=-0.898796 $K_{c\delta1}$=0.005237
K_{cm2}=0.034733 $K_{c\delta2}$=-0.053150

Appendix C

Damping controller designed at P_e=0.8 pu
T_w=10 sec

Damping controller m_1
K_{dc}=182.12, $T_1 = 0.057312$, $T_2 = 0.13174$, $n = 1$

Damping controller m_2
K_{dc}=15.235, $T_1 = 0.083781$, $T_2 = 0.090121$, $n = 1$

Damping controller δ_1
K_{dc}=5.0117, $T_1 = 0.73539$, $T_2 = 0.010267$, $n = 2$

Damping controller δ_2
K_{dc}=34420, $T_1 = 0.00080155$, $T_2 = 9.4198$, $n = 2$